Supporting Information for Publication: Oxygenated Aromatic Compounds are Important Precursors of Secondary Organic Aerosol in Biomass Burning Emissions

Ali Akherati[1], Yicong He[1], Matthew M. Coggon[2,3], Abigail R. Koss[4], Anna L. Hodshire[5], Kanako Sekimoto[2], Carsten Warneke[2,3], Joost de Gouw[6], Lindsay Yee[7], John H. Seinfeld[8], Timothy B. Onasch[9], Scott C. Herndon[9], Walter B. Knighton[10], Christopher D. Cappa[11], Michael J. Kleeman[11], Christopher Y. Lim[4], Jesse H. Kroll[4], Jeffrey R. Pierce[5], and Shantanu H. Jathar[1*]

[1]Department of Mechanical Engineering, Colorado State University, Fort Collins, CO, USA
[2]Cooperative Institute for Research in Environmental Sciences, University of Colorado, Boulder, CO, USA
[3]Chemical Sciences Division, NOAA Earth System Research Laboratory, Boulder, CO, USA
[4]Department of Civil and Environmental Engineering, Massachusetts Institute of Technology, Boston, MA, USA
[5]Department of Atmospheric Science, Colorado State University, Fort Collins, CO, USA
[6]Department of Chemistry and Cooperative Institute for Research in Environmental Sciences, University of Colorado Boulder, Boulder, CO, USA
[7]Environmental Science, Policy, and Management, University of California Berkeley, Berkeley, CA, USA
[8]Department of Chemical Engineering, California Institute of Technology, Pasadena, CA, USA
[9]Aerodyne Research Inc., Billerica, MA, USA
[10]Department of Chemistry, Montana State University, Bozeman, MT, USA
[11]Department of Civil and Environmental Engineering, University of California Davis, Davis, CA, USA
[*]Correspondence to: Shantanu H. Jathar (shantanu.jathar@colostate.edu)

Scaling Factor Calculations

For a few select experiments (Fire001, Fire002, Fire003, Fire004, Fire007, and Fire011), we calculated a scaling factor to correct the raw OA mass concentrations measured by the HR-AMS. Only a few experiments were selected because these were the only experiments where data from the scanning mobility particle sizer (SMPS) was found to be sufficient and not influenced by a second number mode at larger sizes (that prevented complete characterization of the volume concentration and also affected corrections for multiple charges) and synchronization issues between the SMPS and the thermodenuder. The scaling factor is expected to account for losses in the aerodynamic lens, collection efficiency, changes in the relative ionization efficiency, and other potential artifacts associated with the HR-AMS.[1] A mass-based scaling factor was calculated as a ratio of the total non-refractory aerosol mass concentration measured by the HR-AMS (organic+inorganic aerosol) to that estimated from subtracting the black carbon (BC) measured by the single particle soot photometer (SP2) from the mass concentration estimated from the SMPS data. Total aerosol mass concentrations were estimated from the SMPS data by multiplying the volume concentrations by a density of 1.42 g cm^{-3} based on the work of Tkacik et al.[2] Figure S.1 shows that the scaling factor for these select experiments varied inversely with the oxidation state of the OA. This is consistent with the finding of Lim et al.[3] who found the scaling factor to be a function of the OA volatility where the scaling factor was lower for less volatile OA and vice versa. The scaling factor versus oxidation state trends were fit and the fit was used to correct the OA mass concentrations in all experiments.

Table S.1: Fuel, oxidant, and variables of interest (see column headings) for the eleven chamber experiments performed during FIREX. Note that the table is split into three sections for visual clarity, keeping the first two columns the same.

Fire ID	***Fuel***	***Oxidant and precursor***	***Dark period (hr)***	***Lights on (hr)***	***OH exposure (molecules-h cm^{-3})***	***Initial surface area (μm^2 cm^{-3})***
3	Ponderosa pine	OH/HONO	0.13	0.85	3.85×10^6	197
4	Ponderosa pine	OH/H_2O_2	0.34	5.78	7.01×10^6	859
7	Lodgepole pine	OH/HONO	0.98	4.28	1.40×10^7	735
16	Ponderosa pine - litter	UV	0.08	4.13	1.51×10^6	345
22	Douglas-fir - litter	O_3	2.13	2.82	2.27×10^5	269
28	Chaparral (manzanita)	OH/H_2O_2	0.03	5.47	7.20×10^6	306
37	Ponderosa pine	OH/HONO	0.32	3.25	1.22×10^7	413
42	Lodgepole pine	OH/HONO	0.10	4.18	6.38×10^6	287
54	Engelmann spruce	OH/H_2O_2	0.18	2.35	4.14×10^6	117
63	Lodgepole pine	OH/HONO	0.47	2.3	6.28×10^6	182
67	Subalpine fir	O_3	2.18	2.57	3.75×10^5	149

Fire ID	***Fuel***	***Initial OA ($\mu g\ m^{-3}$)***	***Final OA ($\mu g\ m^{-3}$)***	***OA Mass Enh. Ratio***	***Initial O:C Ratio***	***Final O:C Ratio***	***O:C Enh. Ratio***	***Final SOA Mass ($\mu g\ m^{-3}$)***	***Final SOA O:C Ratio***
3	Ponderosa pine	34.4	42.9	1.18	0.22	0.26	1.14	8.5	0.403
4	Ponderosa pine	34.2	79.8	2.17	0.22	0.43	1.92	45.6	0.648
7	Lodgepole pine	35.1	74.4	1.82	0.24	0.38	1.60	39.3	0.548
16	Ponderosa pine - litter	20.4	30.1	1.30	0.19	0.27	1.41	9.7	0.476
22	Douglas-fir - litter	24.5	26.2	1.05	0.31	0.31	0.99	1.7	0.251
28	Chaparral (manzanita)	20.5	26.8	1.37	0.18	0.26	1.46	6.3	0.663
37	Ponderosa pine	60.3	102.2	1.54	0.24	0.35	1.45	42.0	0.558
42	Lodgepole pine	27.3	42.2	1.41	0.25	0.32	1.30	14.9	0.498
54	Engelmann spruce	10.0	12.3	1.22	0.26	0.33	1.26	2.3	0.948
63	Lodgepole pine	17.2	25.0	1.34	0.26	0.34	1.29	7.8	0.566
67	Subalpine fir	15.0	15.4	1.28	0.35	0.36	1.07	0.4	0.850

Fire ID	***Fuel***	***Initial NO (ppbv)***	***Initial NO_2 (ppbv)***	***Initial O_3 (ppbv)***	***Initial NMVOC ($\mu g\ m^{-3}$)***	***Initial NMVOC (ppbv)***	***Initial SOA Precursors ($\mu g\ m^{-3}$)***	***Initial SOA Precursors (ppbv)***
3	Ponderosa pine	2453.7	BDL	6.5	418.1	183.1	166.3	42.6
4	Ponderosa pine	28.7	BDL	11.1	491.1	215.1	195.3	50.1
7	Lodgepole pine	40.3	BDL	5.7	420.0	184.7	160.0	41.1
16	Ponderosa pine - litter	15.1	37.6	6.8	330.8	143.9	124.6	32.2
22	Douglas-fir - litter	25.1	0.05	504.9	30.4	14.4	10.1	2.6
28	Chaparral (manzanita)	21.7	20.2	3.2	168.8	78.0	60.0	15.9
37	Ponderosa pine	318.6	166.7	3.4	191.5	82.4	79.9	20.4
42	Lodgepole pine	346.1	204.5	3.5	143.9	66.2	52.2	13.6
54	Engelmann spruce	2.1	8.4	2.6	94.6	39.8	36.1	9.2
63	Lodgepole pine	294.1	249.7	4.0	222.3	102.4	80.6	21.1
67	Subalpine fir	0.04	8.8	436.7	217.5	96.0	84.4	21.4

Table S.2: Emissions ratios of SOA precursors with acetonitrile (g g^{-1}) used to calculate SOA precursor concentrations in the 11 chamber experiments.

Emissions Profile	***Based on?***	***Biogenics***	***Oxygenated Aromatics***	***Heterocyclics***	***Reduced Aromatics***	***Alkanes + Partially Speciated***
Fire003 - this study	Average of Fire 001, 002, 037, 059, 072	12.5	19.3	30.1	15.9	15.2
Fire003 - Sekimoto et al.		9.0	20.9	36.4	19.0	1.5
Fire003 - Koss et al.	All Fires	8.3	15.5	24.8	11.9	15.0
Fire004 - this study	Average of fires 001, 002, 037, 059, 072	12.8	19.3	30.1	15.9	15.2
Fire004 - Sekimoto et al.		9.2	20.9	36.4	19.0	1.5
Fire004 - Koss et al.	All Fires	8.4	15.5	24.8	11.9	15.0
Fire007 - this study	Fire007	8.1	22.7	30.7	18.0	19.7
Fire007 - Sekimoto et al.		7.7	25.2	41.6	17.8	2.0
Fire007 - Koss et al.	All Fires	8.3	15.5	24.8	11.9	19.3
Fire016 - this study	Fire038	3.9	18.0	37.6	9.8	16.8
Fire016 - Sekimoto et al.		7.4	28.0	44.9	17.0	2.2
Fire016 - Koss et al.	All Fires	8.8	15.5	24.8	11.9	15.5
Fire022 - this study	Average of fires 014, 018, 031, 043, 057, 064	0.7	19.4	26.6	15.7	13.4
Fire022 - Sekimoto et al.		0.9	23.8	39.9	18.2	1.8
Fire022 - Koss et al.	All Fires	0.6	15.5	24.8	11.9	3.2
Fire028 - this study	Fire028	4.1	23.5	38.8	23.8	18.1
Fire028 - Sekimoto et al.		8.7	24.8	41.1	17.9	1.9
Fire028 - Koss et al.	All Fires	9.0	15.5	24.8	11.9	18.2
Fire037 - this study	Fire037	14.6	24.4	36.0	19.9	15.6
Fire037 - Sekimoto et al.		9.6	20.4	35.9	19.1	1.5
Fire037 - Koss et al.	All Fires	8.6	15.5	24.8	11.9	15.2
Fire042 - this study	Average of Fires 006, 007, 058, 063	9.3	16.6	25.8	16.6	15.1
Fire042 - Sekimoto et al.		9.5	21.7	37.4	18.8	1.6
Fire042 - Koss et al.	All Fires	8.8	15.5	24.8	11.9	15.1
Fire054 - this study	Fire008	2.0	12.5	17.0	6.6	11.4
Fire054 - Sekimoto et al.		8.6	24.1	40.3	18.1	1.8
Fire054 - Koss et al.	All Fires	8.8	15.5	24.8	11.9	11.4
Fire063 - this study	Fire063	8.6	16.8	28.1	16.7	15.9
Fire063 - Sekimoto et al.		8.9	22.3	38.2	18.6	1.7
Fire063 - Koss et al.	All Fires	8.5	15.5	24.8	11.9	15.8
Fire067 - this study	Fire067	1.2	27.4	39.1	25.7	24.7
Fire067 - Sekimoto et al.		0.9	27.1	43.9	17.2	2.2
Fire067 - Koss et al.	All Fires	0.7	15.5	24.8	11.9	24.3

Table S.3: VOC species measured by the PTR-ToF-MS (Koss et al.[10]) and considered as SOA precursors in our model.

Species name	***Species formula***	***k_{OH} [cm^3 molecules^{-1} s^{-1}]***	***Cstar [µg m^{-3}]***	***MW [g mol^{-1}]***	***Surrogate***
Pyrrole	C4H5N	1.45×10^{-10}	5.74×10^{7}	67.0892	Heterocyclics
Furan	C4H4O	4.00×10^{-11}	2.23×10^{9}	68.07356	Heterocyclics
Isoprene	C5H8	1.00×10^{-10}	2.05×10^{9}	68.11702	Biogenics
Dihydropyrrole	C4H7N	1.04×10^{-10}	5.15×10^{7}	69.10508	Heterocyclics
Tetrahydropyrrole	C4H9N	7.85×10^{-11}	2.44×10^{8}	71.12096	Heterocyclics
Benzene	C6H6	1.22×10^{-12}	4.05×10^{8}	78.11184	Aromatics
Pyridine	C5H5N	3.70×10^{-13}	5.28×10^{7}	79.0999	Heterocyclics
Methylpyrrole	C5H7N	1.10×10^{-10}	5.69×10^{7}	81.11578	Heterocyclics
MethylFuran	C5H6O	7.80×10^{-11}	7.71×10^{8}	82.10014	Heterocyclics
Thiophene	C4H4S	9.53×10^{-12}	3.64×10^{8}	84.13956	Heterocyclics
Furanone	C4H4O2	5.66×10^{-11}	1.34×10^{7}	84.07256	Heterocyclics
Ethynylpyrrole	C6H5N	6.45×10^{-11}	3.95×10^{6}	92.11854	Heterocyclics
Toluene	C7H8	5.63×10^{-12}	1.42×10^{8}	92.13842	Aromatics
2-Furancarbonitrile	C5H3NO	7.15×10^{-12}	1.81×10^{5}	93.08302	Heterocyclics
MethylPyridine	C6H7N	1.10×10^{-12}	4.36×10^{7}	93.12648	Heterocyclics
Phenol	C6H6O	2.80×10^{-11}	2.11×10^{6}	94.11084	Oxygenated Aromatics
4-Pyridinol	C5H5NO	7.65×10^{-11}	1.81×10^{5}	95.0989	Heterocyclics
C2-pyrroles	C6H9N	2.00×10^{-10}	4.16×10^{6}	95.14236	Heterocyclics
Furfural	C5H4O2	3.56×10^{-11}	1.14×10^{7}	96.08326	Heterocyclics
Dimethylfuran	C6H8O	2.00×10^{-10}	1.40×10^{7}	96.12672	Heterocyclics
Methylthiophene	C5H6S	9.51×10^{-12}	1.28×10^{8}	98.16614	Heterocyclics
2Methanolfuran	C5H6O2	1.04×10^{-10}	3.88×10^{6}	98.09914	Heterocyclics
Dihydrofurandione	C4H4O3	8.56×10^{-13}	9.00×10^{3}	100.0716	Heterocyclics
Phenylacetylene	C8H6	8.02×10^{-12}	2.16×10^{6}	102.1332	Aromatics
Benzonitrile	C7H5N	3.44×10^{-13}	4.62×10^{6}	103.1213	Aromatics
Styrene	C8H8	5.80×10^{-11}	3.43×10^{7}	104.1491	Aromatics
Vinylpyridine	C7H7N	2.66×10^{-11}	1.55×10^{6}	105.1372	Heterocyclics
Benzaldehyde	C7H6O	1.20×10^{-11}	7.30×10^{6}	106.1215	Aromatics
C8_Aromatics	C8H10	1.32×10^{-11}	4.88×10^{7}	106.165	Aromatics
PyridineAldehyde	C6H5NO	1.71×10^{-11}	7.85×10^{4}	107.1096	Heterocyclics
Dimethylpyridine	C7H9N	2.79×10^{-12}	2.05×10^{7}	107.1531	Heterocyclics
Benzoquinone	C6H4O2	4.51×10^{-12}	8.80×10^{5}	108.094	Aromatics
Cresol	C7H8O	5.30×10^{-11}	1.34×10^{7}	108.1374	Oxygenated Aromatics
Trimethylpyrrole	C7H11N	2.00×10^{-10}	1.20×10^{7}	109.1689	Heterocyclics
Benzenediol	C6H6O2	1.04×10^{-10}	1.10×10^{6}	110.1098	Oxygenated Aromatics
Trimethylfuran	C7H10O	1.59×10^{-10}	9.27×10^{7}	110.1533	Heterocyclics
Dihydroxypyridine	C5H5NO2	4.55×10^{-11}	3.78×10^{4}	111.0979	Heterocyclics
5-Hydroxy 2-furfural	C5H4O3	4.90×10^{-11}	7.36×10^{5}	112.0823	Heterocyclics
Nitrofuran	C4H3NO3	5.06×10^{-12}	1.64×10^{4}	113.0703	Heterocyclics
5-hydroxymethyl-	C5H6O3	1.00×10^{-10}	2.59E+0^{5}	114.0981	Heterocyclics

2[3H]-furanone					
5-hydroxy tetrahydro 2-furfural	C5H8O3	5.00×10^{-12}	7.36×10^{5}	116.114	Heterocyclics
Indene	C9H8	7.80×10^{-11}	1.06×10^{7}	116.1598	Aromatics
Benzeneacetonitrile	C8H7N	2.07×10^{-12}	5.72×10^{5}	117.1479	Aromatics
Benzofuran	C8H6O	3.70×10^{-11}	1.13×10^{7}	118.1322	Aromatics
Methylstyrene	C9H10	5.40×10^{-11}	1.14×10^{7}	118.1757	Aromatics
Isoindoline	C8H9N	8.00×10^{-11}	6.08×10^{5}	119.1638	Heterocyclics
Tolualdehyde	C8H8O	1.60×10^{-11}	2.39×10^{6}	120.1481	Aromatics
C9_Aromatics	C9H12	2.20×10^{-11}	1.95×10^{7}	120.1916	Aromatics
Salicylaldehyde	C7H6O2	2.80×10^{-11}	3.72×10^{6}	122.1205	Aromatics
Dimethylphenol	C8H10O	5.05×10^{-11}	5.31×10^{6}	122.164	Oxygenated Aromatics
Nitrobenzene	C6H5NO2	1.40×10^{-13}	1.50×10^{6}	123.1086	Aromatics
Hydroxy benzoquinone	C6H4O3	1.30×10^{-11}	4.11×10^{5}	124.093	Aromatics
Guaiacol	C7H8O2	7.53×10^{-11}	9.16×10^{5}	124.1364	Oxygenated Aromatics
Hydroxymethylfurfural	C6H6O3	1.00×10^{-10}	4.11×10^{5}	126.1088	Heterocyclics
Dihydroxymethylfuran	C6H8O3	1.29×10^{-10}	4.11×10^{5}	128.1247	Heterocyclics
Naphthalene	C10H8	2.30×10^{-11}	5.73×10^{5}	128.1705	Aromatics
dihydronaphthalene	C10H10	6.42×10^{-11}	5.11×10^{6}	130.1864	Aromatics
Methylindole	C9H9N	2.00×10^{-10}	3.64×10^{4}	131.1745	Aromatics
Methyl benzofuran	C9H8O	9.75×10^{-11}	3.54×10^{6}	132.1588	Heterocyclics
Methyl propenyl benzene	C10H12	3.30×10^{-11}	6.76×10^{6}	132.2023	Aromatics
3-methylacetophenone	C9H10O	2.42×10^{-12}	1.60×10^{6}	134.1747	Aromatics
C10_Aromatics	C10H14	9.50×10^{-12}	1.04×10^{7}	134.2182	Aromatics
Methylbenzoicacid	C8H8O2	1.20×10^{-11}	1.66×10^{4}	136.1471	Aromatics
Monoterpenes	C10H16	1.63×10^{-10}	2.16×10^{7}	136.234	Biogenics
Nitrotoluene	C7H7NO2	7.72×10^{-13}	5.96×10^{5}	137.1352	Aromatics
MethylGuaiacol	C8H10O2	3.98×10^{-11}	5.62×10^{5}	138.163	Oxygenated Aromatics
Methylnaphthalene	C11H10	5.65×10^{-11}	5.20×10^{5}	142.1971	Aromatics
Product of levoglucosan dehydration (pyrolysis)	C6H8O4	5.28×10^{-11}	3.81×10^{4}	144.1237	Alkanes
Naphthol	C10H8O	2.00×10^{-10}	2.71×10^{5}	144.1695	Aromatics
Ethylindene	C11H12	6.36×10^{-11}	1.67×10^{6}	144.213	Aromatics
Dimethylbenzofuran	C10H10O	1.20×10^{-10}	2.71×10^{5}	146.1854	Aromatics
Methylchavicol	C10H12O	5.43×10^{-11}	1.13×10^{6}	148.2013	Oxygenated Aromatics
C11_aromatics	C11H16	5.00×10^{-11}	4.81×10^{6}	148.2447	Aromatics
VinylGuaiacol	C9H10O2	5.44×10^{-11}	2.28×10^{5}	150.1737	Oxygenated

					Aromatics
Vanillin	C8H8O3	2.73×10^{-11}	7.00×10^{5}	152.1461	Oxygenated Aromatics
Acenaphthylene	C12H8	7.55×10^{-11}	6.18×10^{4}	152.1919	Aromatics
Camphor	C10H16O	4.30×10^{-12}	1.98×10^{6}	152.233	Biogenics
Syringol	C8H10O3	9.66×10^{-11}	1.00×10^{5}	154.162	Oxygenated Aromatics
Cineole	C10H18O	2.26×10^{-11}	1.63×10^{7}	154.2489	Biogenics
1,3-dimethylnaphthalene	C12H12	6.94×10^{-11}	8.57×10^{4}	156.2237	Aromatics
Decanal	C10H20O	3.45×10^{-11}	1.27×10^{6}	156.2648	Alkanes
C12_aromatics	C12H18	1.13×10^{-10}	1.17×10^{6}	162.2713	Aromatics
Isoeugenol	C10H12O2	8.84×10^{-11}	1.94×10^{5}	188.2217	Oxygenated Aromatics
C13_aromatics	C13H20	1.13×10^{-10}	7.17×10^{5}	176.2979	Aromatics
Sesquiterpenes	C15H24	3.00×10^{-10}	4.58×10^{4}	204.3511	Biogenics
5-Methyl furfural	C6H6O2	5.18×10^{-11}	1.10×10^{6}	110.1098	Heterocyclics

Table S.4: SOM grids, surrogates, and parameters used in this work.

Precursor Class	***VOC Surrogate***	***ΔLVP***	m_{frag}	p_{1O}	p_{2O}	p_{3O}	p_{4O}	***Reference***
Long alkanes	*n*-dodecane	1.4629	0.2627	0.9657	0.0010	0.0020	0.0314	Loza et al.[4]
Benzene	benzene	1.5495	0.7895	0.0743	0.0213	0.8963	0.0081	Ng et al.[5]
Toluene	toluene	1.4169	1.3064	0.5634	0.3413	0.0016	0.0937	Zhang et al.[6]
C_{8+} single-ring aromatics	*m*-xylene	1.4601	0.0736	0.1418	0.2971	0.4571	0.1040	Ng et al.[5]
Polycyclic aromatic hydrocarbons (PAH)	naphthalene	1.4922	0.7673	0.8138	0.0072	0.0635	0.1155	Zhang et al.[6]
Isoprene	isoprene	1.8742	0.5207	0.9924	0.0003	0.0065	0.0009	Chhabra et al.[7]
Terpene	α-pinene	1.9139	0.1312	0.5991	0.2923	0.1079	0.0007	Chhabra et al.[7]
Oxygenated aromatics	phenol, guaiacol	2.023	0.315	0.109	0.048	0.439	0.404	Yee et al.[8]
Oxygenated aromatics	syringol	1.629	0.148	0.394	0.121	0.071	0.414	Yee et al.[8]
Heterocyclic compounds	2-methylfuran, dimethylfuran	1.459	0.449	0.0005	0.0014	0.998	0.0001	He et al.[9]

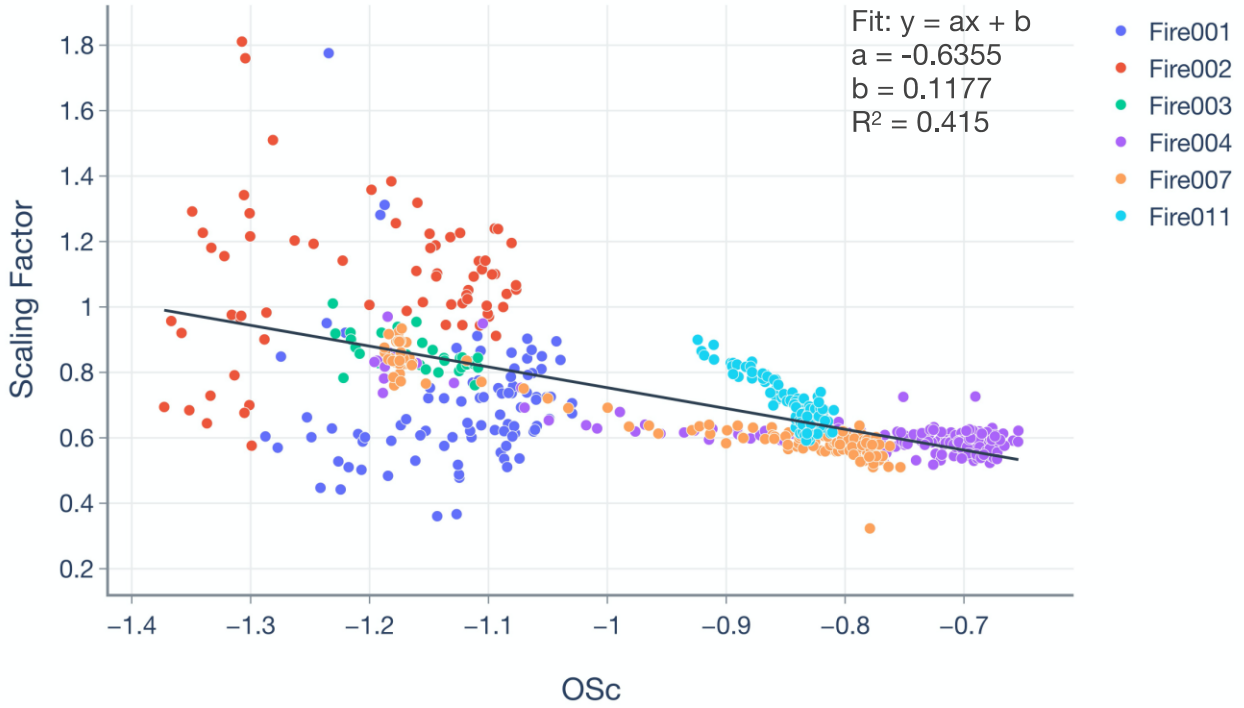

Figure S.1: Scaling factor (SF) as a function of the oxidation state (OSc) for six different experiments. The OSc was approximated as 2×O:C-H:C.[11] The relatively larger variability in SF for Fire001 and Fire002 can be attributed to low initial OA mass concentrations in those experiments (<4 µg m^{-3}) compared to the rest (>20 µg m^{-3}). Gas-phase data were unavailable for Fire001 and Fire002 and hence were not modeled in this study. Fire011 was a nitrate (NO_3) radical experiment performed in the dark and the oxidation results from that experiment will be discussed in a companion paper.

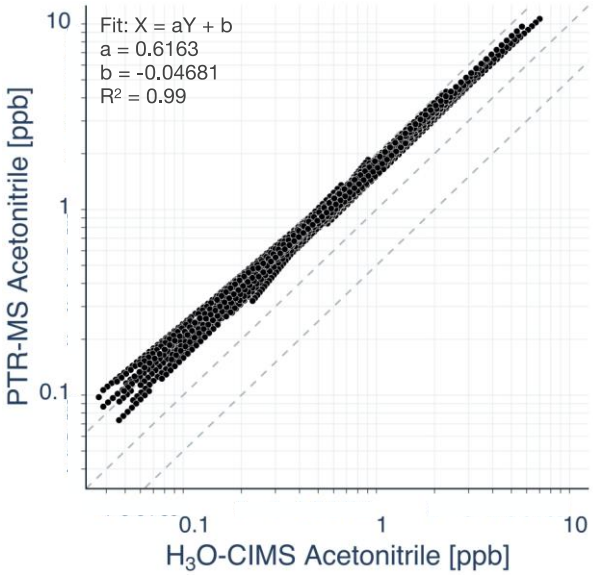

Figure S.2: Scatter plot comparing the acetonitrile concentration measured by the PTR-MS and PTR-ToF-MS in the MIT/UCD mini-chamber over 30 experiments.[2] The slope was used to correct the acetonitrile concentrations in the CSU chamber before being used to determine the initial concentrations of SOA precursors.

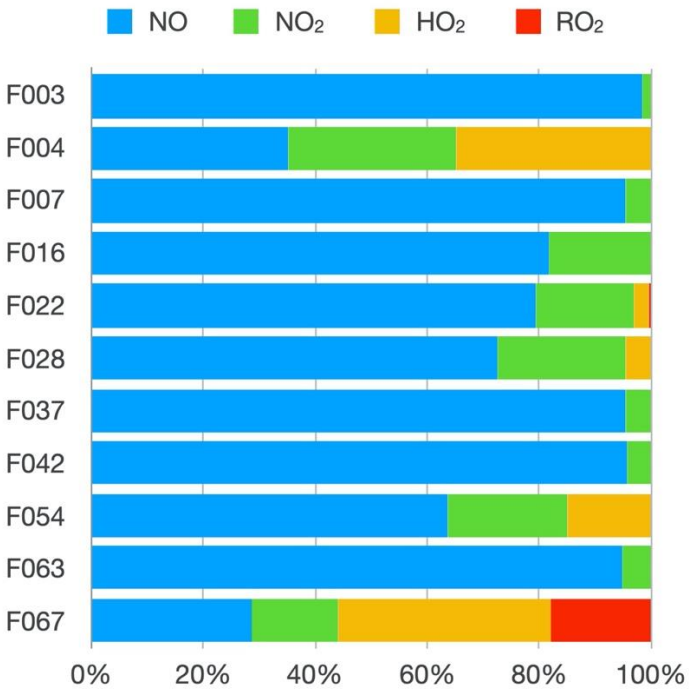

Figure S.3: Averaged fate of the RO_2 radical with reaction with NO, NO_2, HO_2, and RO_2, based on predictions from the Master Chemical Mechanism (MCM) over the entire duration of the chamber experiment.[12] Here, we only calculated the fate of RO_2 radicals with a carbon number larger than or equal to 4.

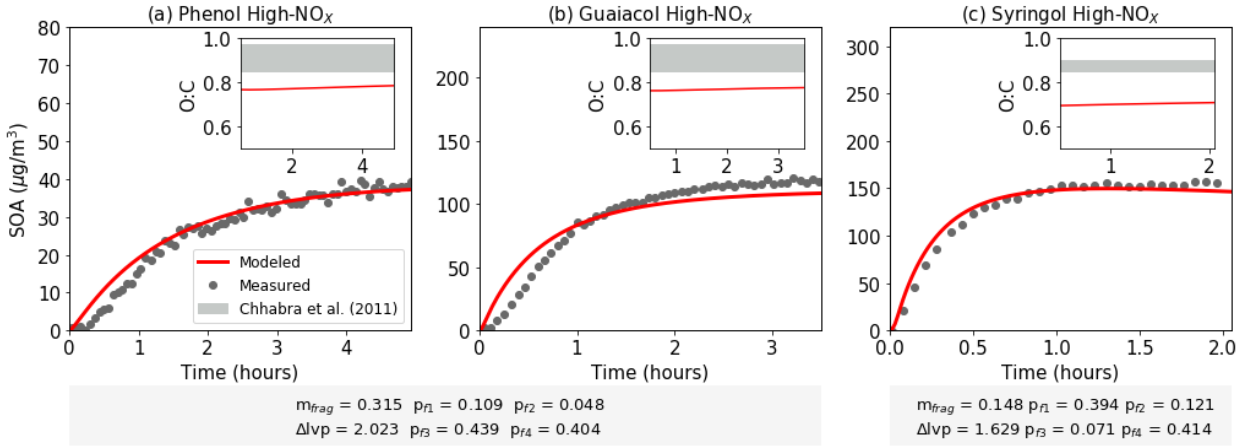

Figure S.4: Model predictions of SOA mass concentrations and O:C ratios for (a) phenol, (b) guaiacol, and (c) syringol compared against measurements from Yee et al.[8] and Chhabra et al.[7]

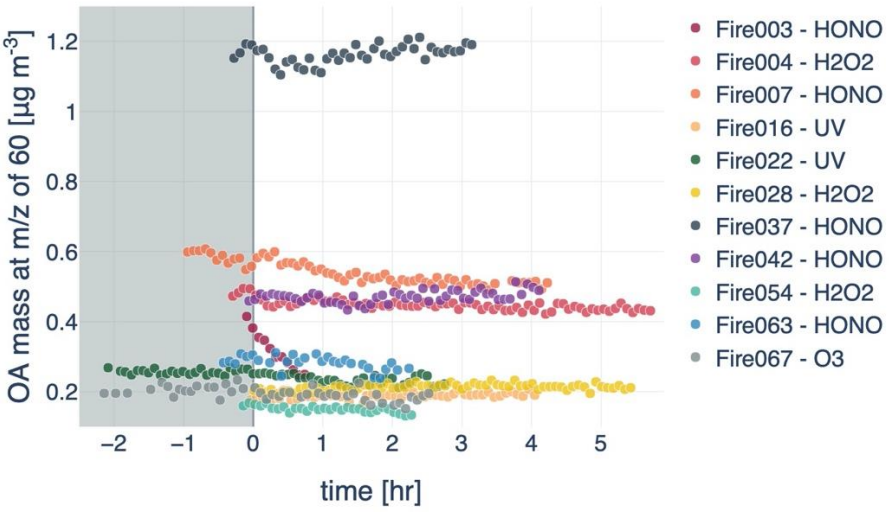

Figure S.5: Particle-wall-loss-corrected OA mass concentrations measured by the HR-AMS at a mass-to-charge ratio of 60.02113 for all eleven chamber experiments. Except for Fire003, the mass was found to be relatively constant during the lights-on period of the experiment, which we concluded as little indication of oxidation of POA.

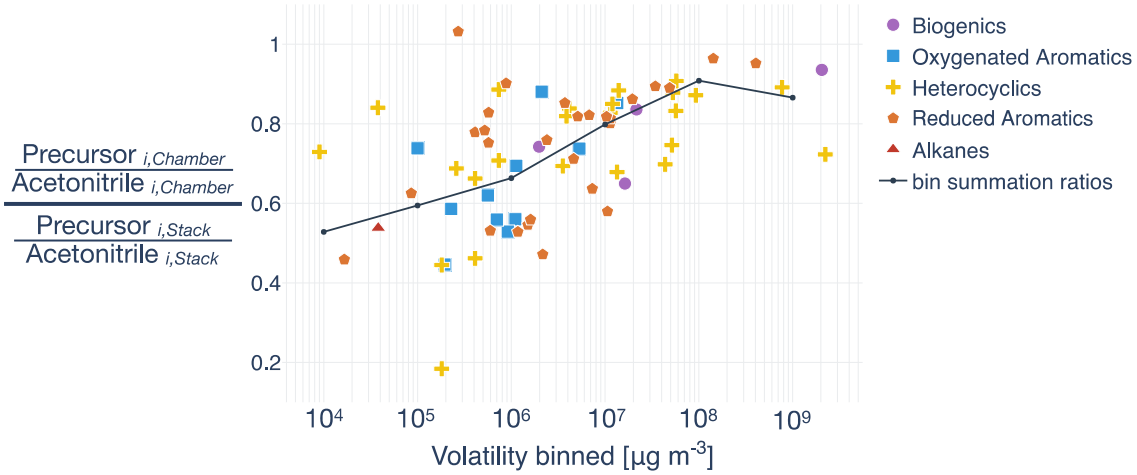

Figure S.6: Emissions ratios of individual SOA precursors to acetonitrile ratioed between those measured in the chamber to those measured in the stack for Fire007. The data are resolved by SOA precursor class. A ratio of 1 indicates no loss in the transfer duct and a ratio of 0 indicates a complete loss in the transfer duct. The time series of these species in the chamber were relatively flat during the dark period indicating that the losses were from those in the transfer duct and not to the walls of the chamber. The solid black line represents the chamber-to-stack ratio if the species were binned by volatility.

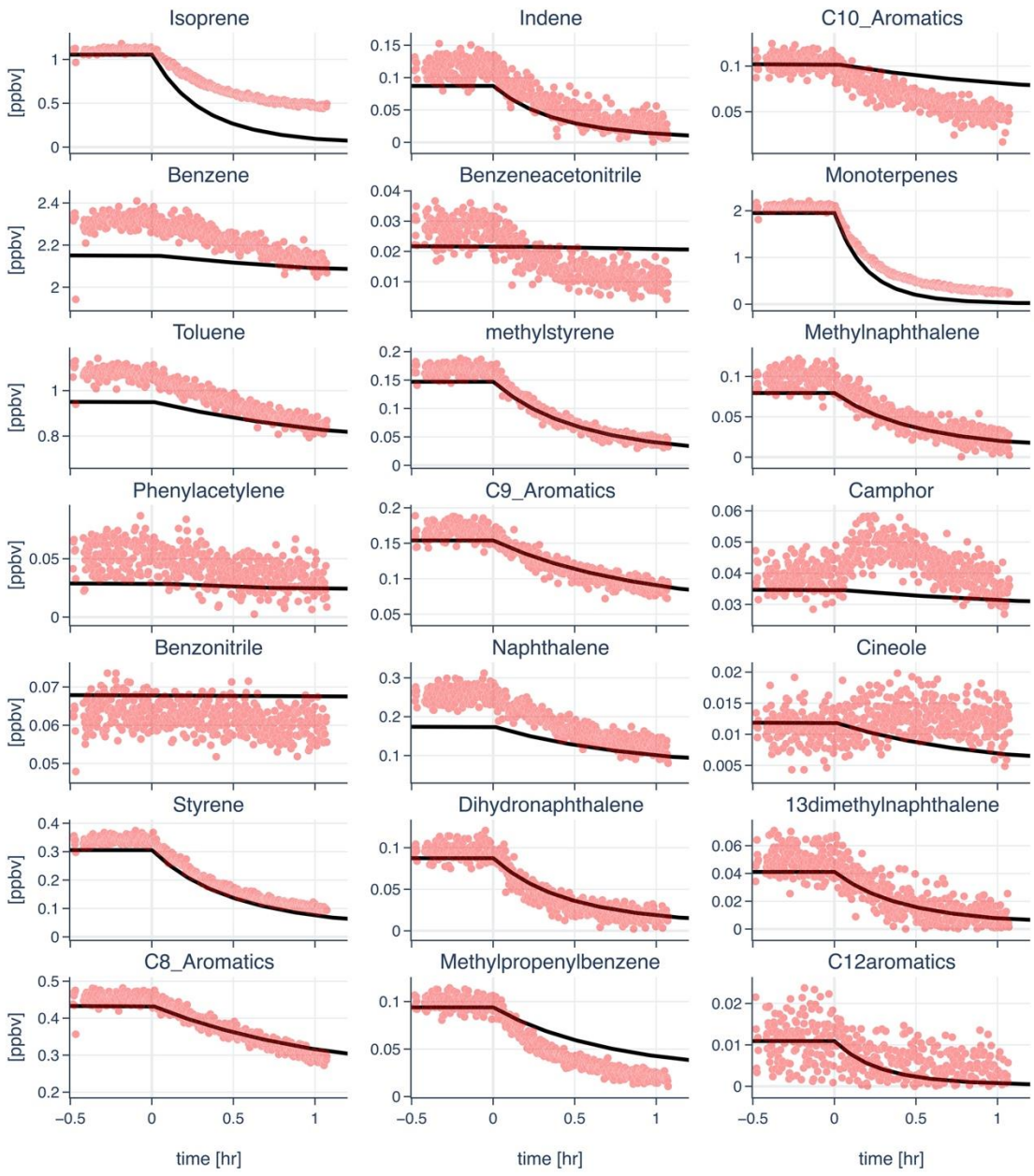

Figure S.7: Modeled (solid black line) and measured (peach circles) decay of reduced hydrocarbons identified by the PTR-ToF-MS for the chamber experiments performed on Fire007.

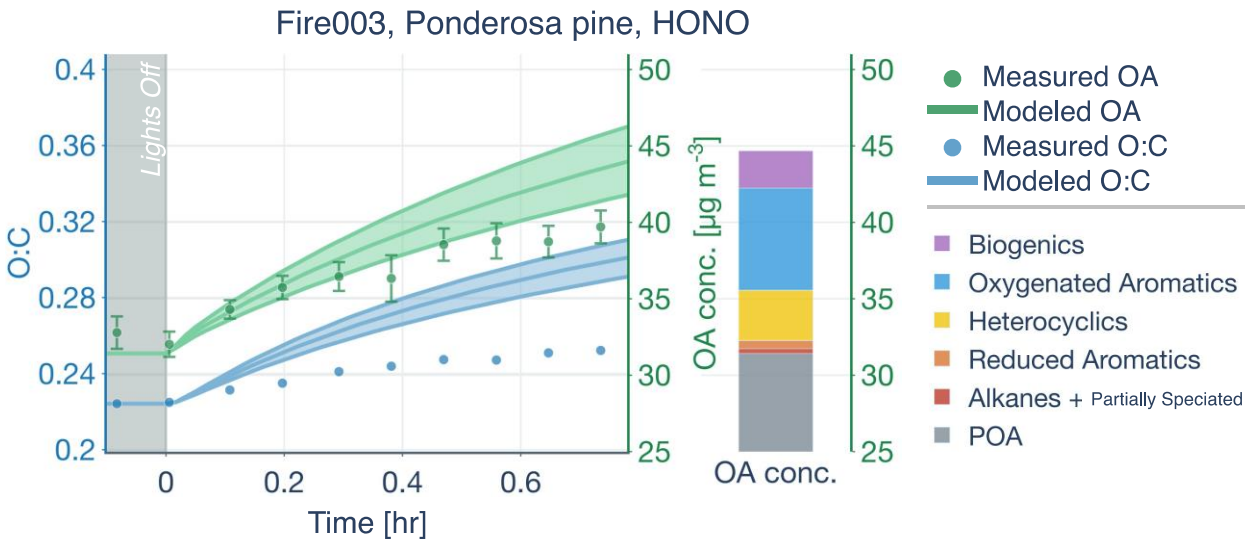

Figure S.8: Model predictions of OA mass concentrations (solid green line) and O:C ratio (solid blue line) compared with measurements (filled circles, same color scheme) for a Ponderosa pine experiment performed at high NO_X conditions (Fire003). The bar to the right shows the modeled contributions of POA and precursor-resolved SOA to the end-of-experiment OA.

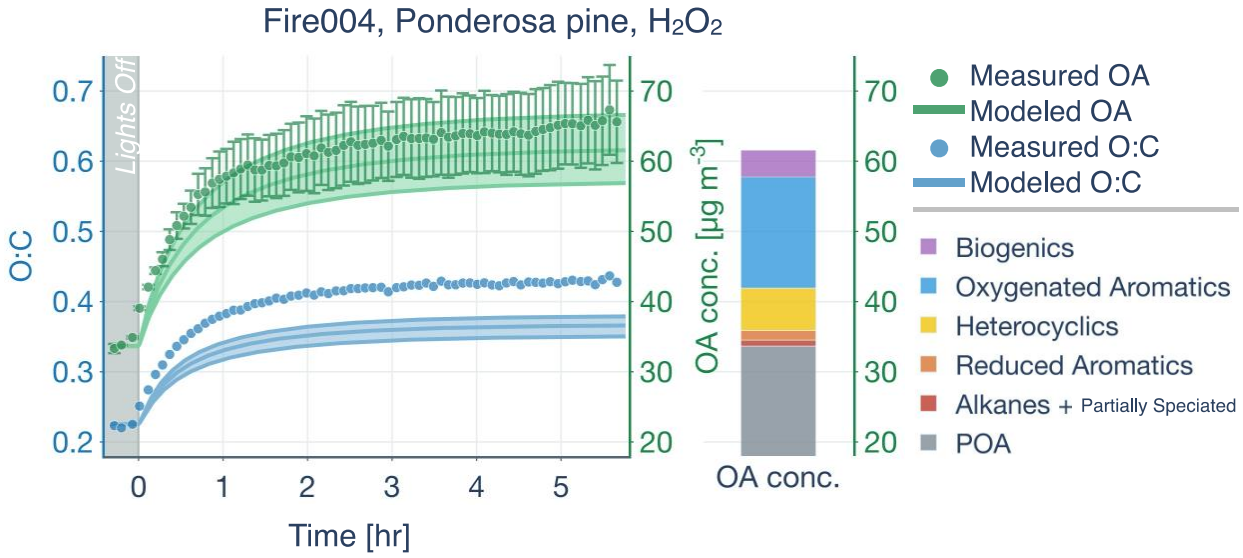

Figure S.9: Model predictions of OA mass concentrations (solid green line) and O:C ratio (solid blue line) compared with measurements (filled circles, same color scheme) for a Ponderosa pine experiment performed at high NO_X conditions (Fire004). The bar to the right shows the modeled contributions of POA and precursor-resolved SOA to the end-of-experiment OA.

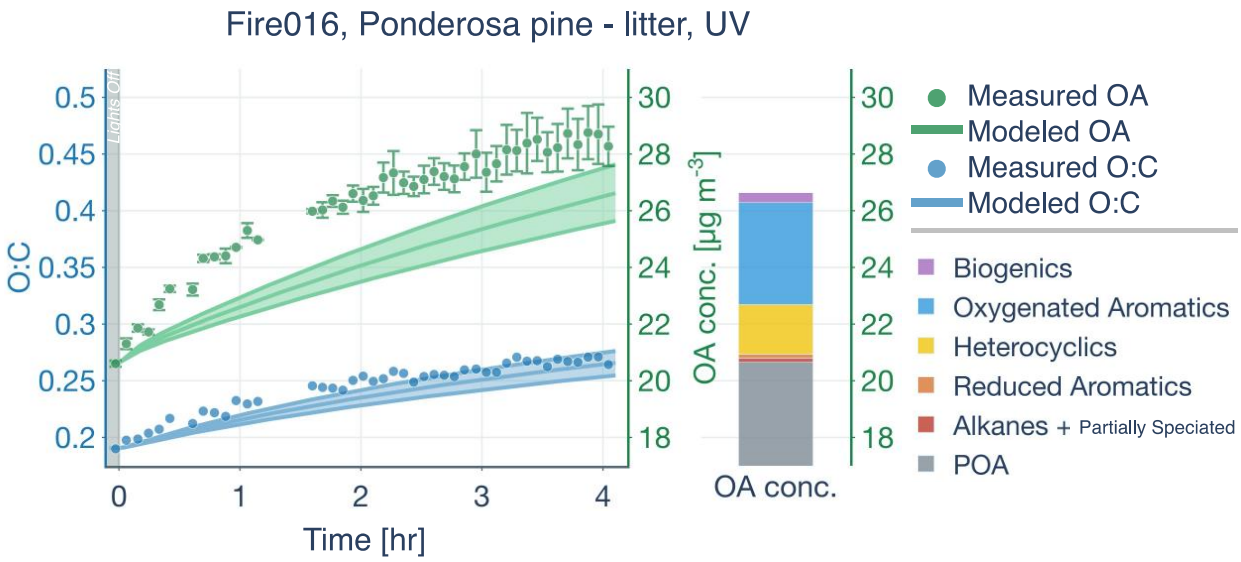

Figure S.10: Model predictions of OA mass concentrations (solid green line) and O:C ratio (solid blue line) compared with measurements (filled circles, same color scheme) for a Ponderosa pine experiment performed without added oxidants (Fire016). The bar to the right shows the modeled contributions of POA and precursor-resolved SOA to the end-of-experiment OA.

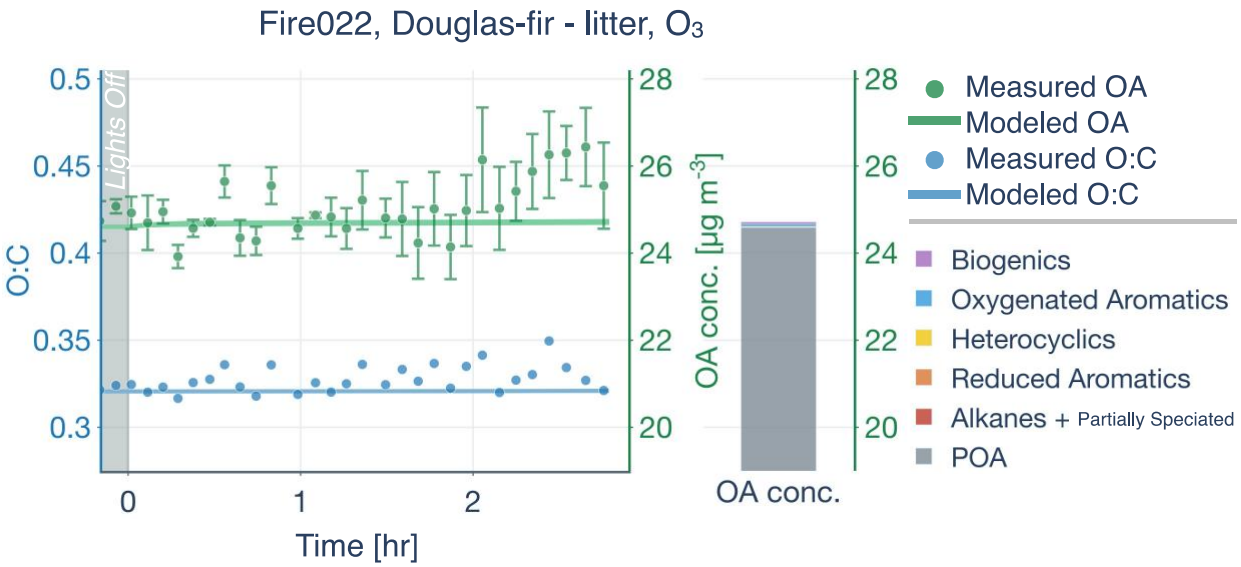

Figure S.11: Model predictions of OA mass concentrations (solid green line) and O:C ratio (solid blue line) compared with measurements (filled circles, same color scheme) for a Douglas fir experiment performed without added oxidants (Fire022). The bar to the right shows the modeled contributions of POA and precursor-resolved SOA to the end-of-experiment OA.

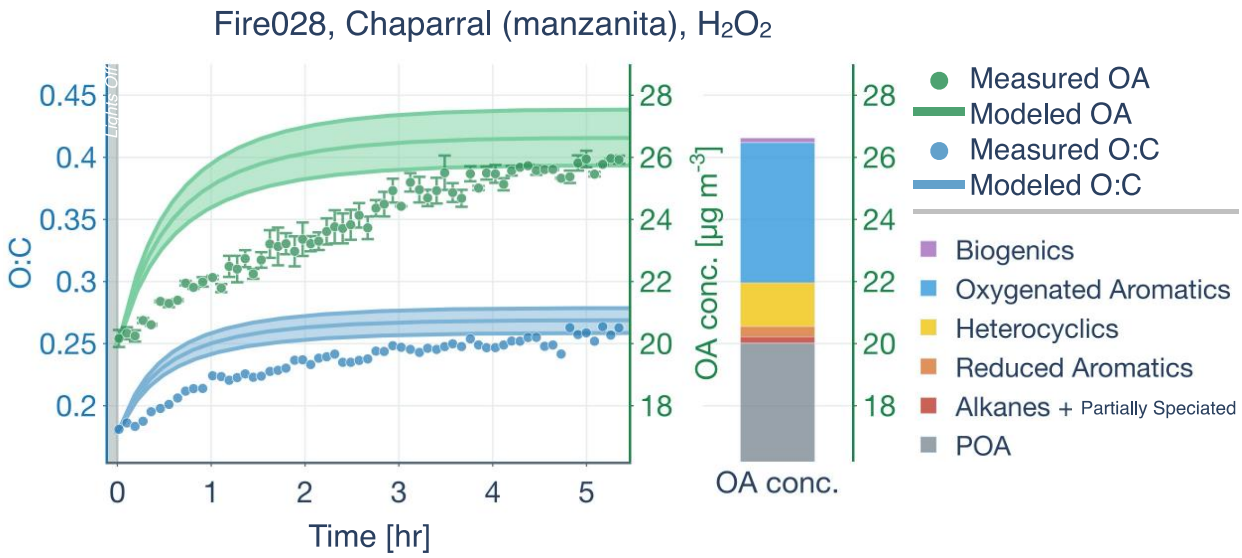

Figure S.12: Model predictions of OA mass concentrations (solid green line) and O:C ratio (solid blue line) compared with measurements (filled circles, same color scheme) for a chaparral (manzanita) experiment performed at high NO_X conditions (Fire028). The bar to the right shows the modeled contributions of POA and precursor-resolved SOA to the end-of-experiment OA.

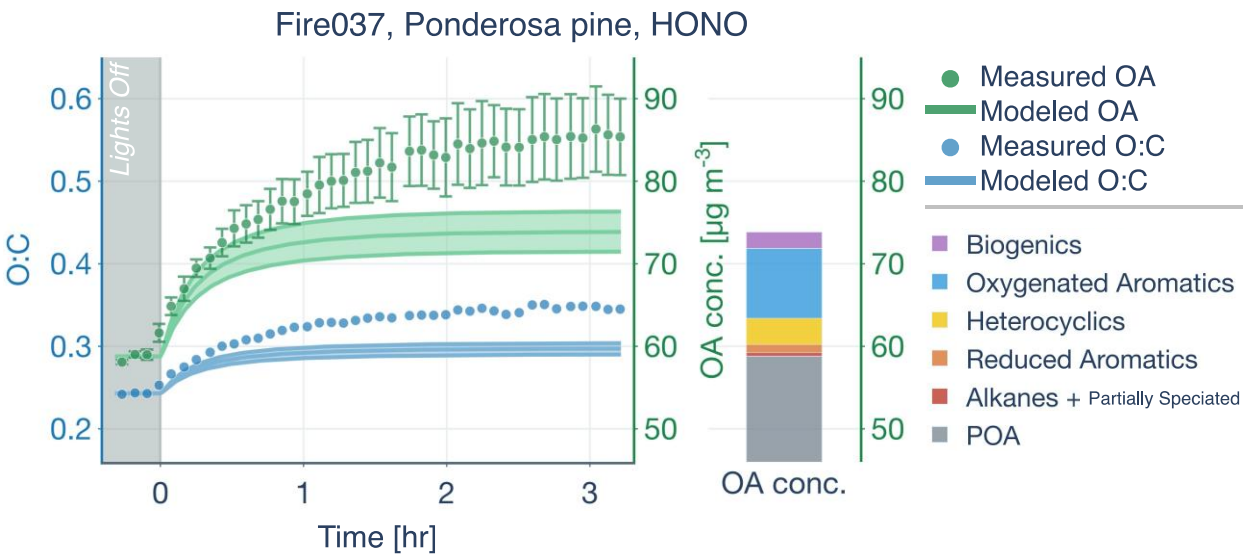

Figure S.13: Model predictions of OA mass concentrations (solid green line) and O:C ratio (solid blue line) compared with measurements (filled circles, same color scheme) for a Ponderosa pine experiment performed at high NO_X conditions (Fire037). The bar to the right shows the modeled contributions of POA and precursor-resolved SOA to the end-of-experiment OA.

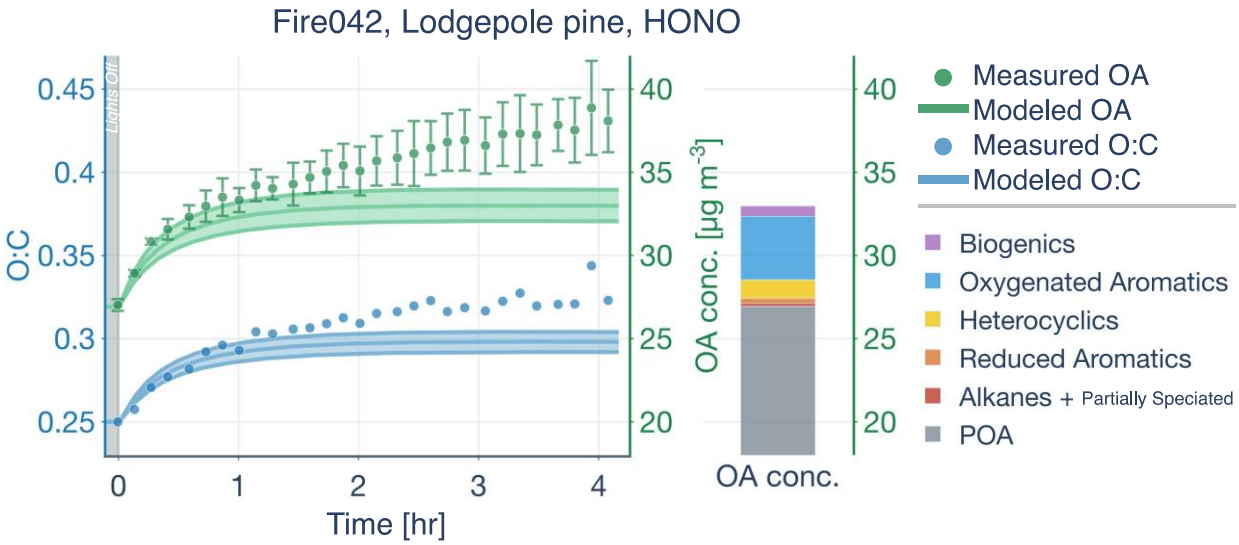

Figure S.14: Model predictions of OA mass concentrations (solid green line) and O:C ratio (solid blue line) compared with measurements (filled circles, same color scheme) for a Lodgepole pine experiment performed at high NO_X conditions (Fire042). The bar to the right shows the modeled contributions of POA and precursor-resolved SOA to the end-of-experiment OA.

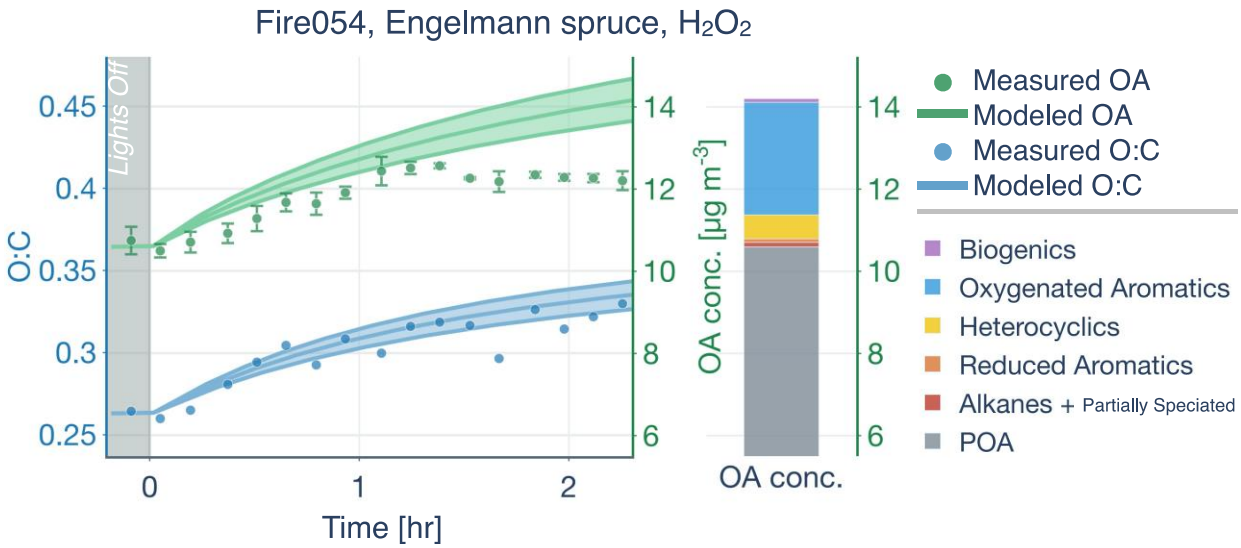

Figure S.15: Model predictions of OA mass concentrations (solid green line) and O:C ratio (solid blue line) compared with measurements (filled circles, same color scheme) for an Engelmann spruce experiment performed at high NO_X conditions (Fire054). The bar to the right shows the modeled contributions of POA and precursor-resolved SOA to the end-of-experiment OA.

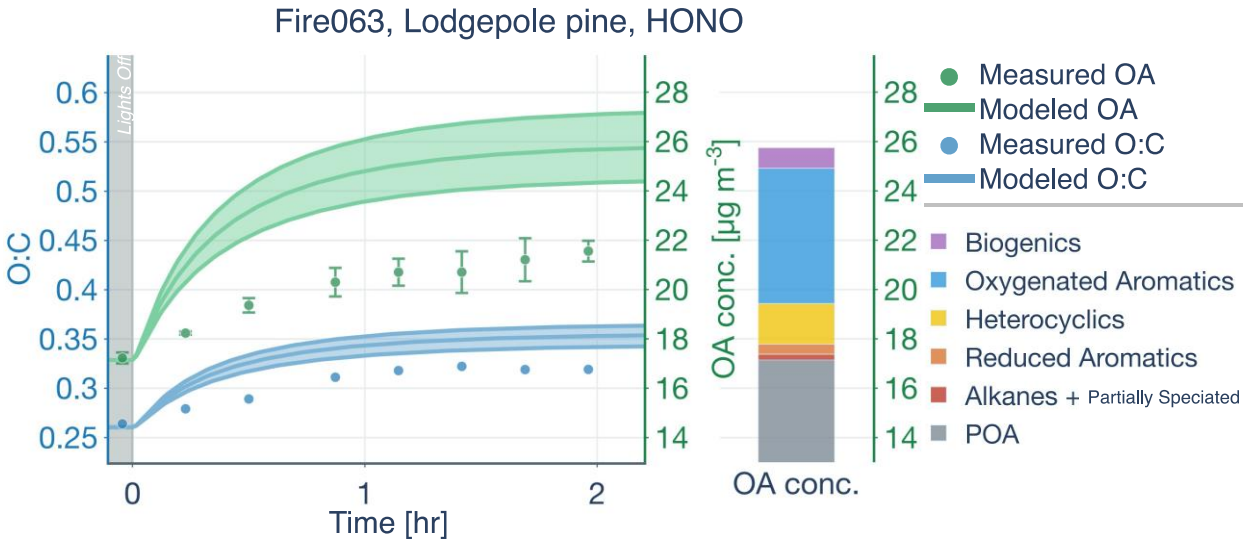

Figure S.16: Model predictions of OA mass concentrations (solid green line) and O:C ratio (solid blue line) compared with measurements (filled circles, same color scheme) for a Lodgepole pine experiment performed at high NO_X conditions (Fire063). The bar to the right shows the modeled contributions of POA and precursor-resolved SOA to the end-of-experiment OA.

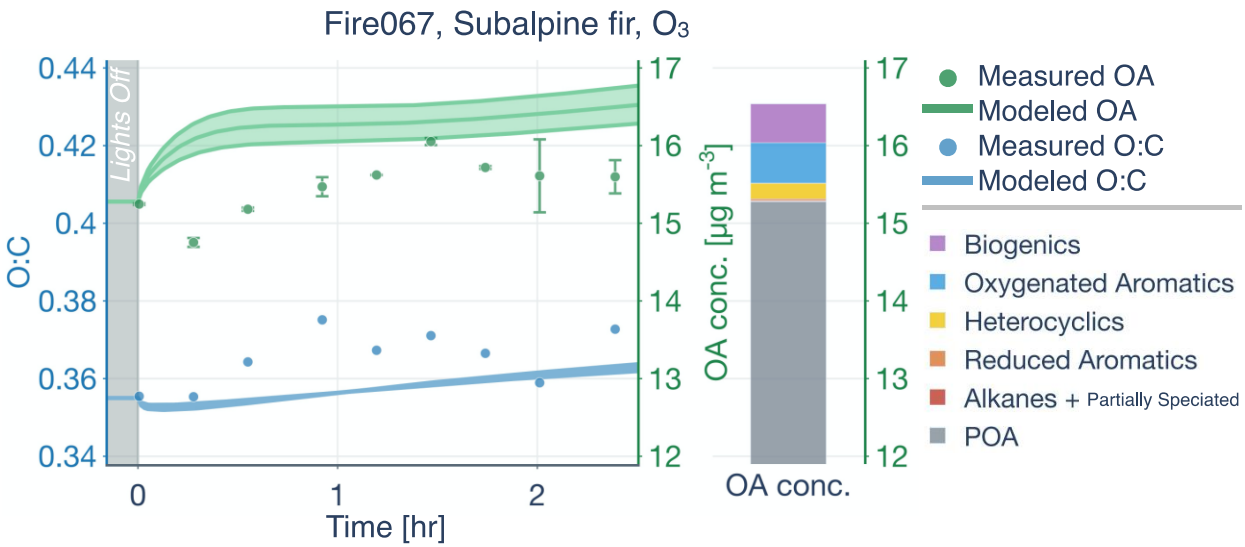

Figure S.17: Model predictions of OA mass concentrations (solid green line) and O:C ratio (solid blue line) compared with measurements (filled circles, same color scheme) for a subalpine fir experiment performed with additional ozone (Fire067). The bar to the right shows the modeled contributions of POA and precursor-resolved SOA to the end-of-experiment OA.

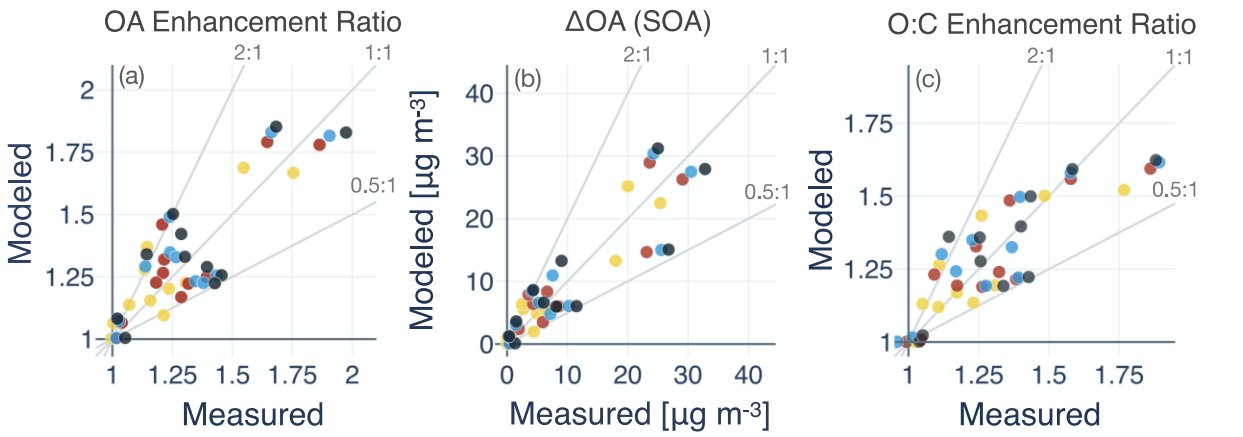

	time	Slope	intercept	R^2	RMSE	Slope	intercept	R^2	RMSE	Slope	intercept	R^2	RMSE
●	25%	0.88	0.18	0.79	0.111	0.91	0.96	0.89	3.01	0.69	0.37	0.72	0.103
●	50%	0.91	0.13	0.78	0.126	0.88	0.98	0.86	3.81	0.70	0.37	0.77	0.101
●	75%	0.86	0.21	0.73	0.145	0.83	1.41	0.82	4.53	0.67	0.43	0.75	0.106
●	100%	0.79	0.29	0.68	0.161	0.80	1.62	0.79	4.97	0.70	0.38	0.69	0.122

Figure S.18: Model-measurement comparison for (a) OA mass enhancement ratios (ratio of final to initial particle-wall-loss-corrected OA mass), (b) SOA production (µg m^{-3}), and (c) OA O:C enhancement ratios (ratio of final to initial O:C ratios) for all eleven chamber experiments at four different time percentiles: 25%, 50%, 75%, and 100%.

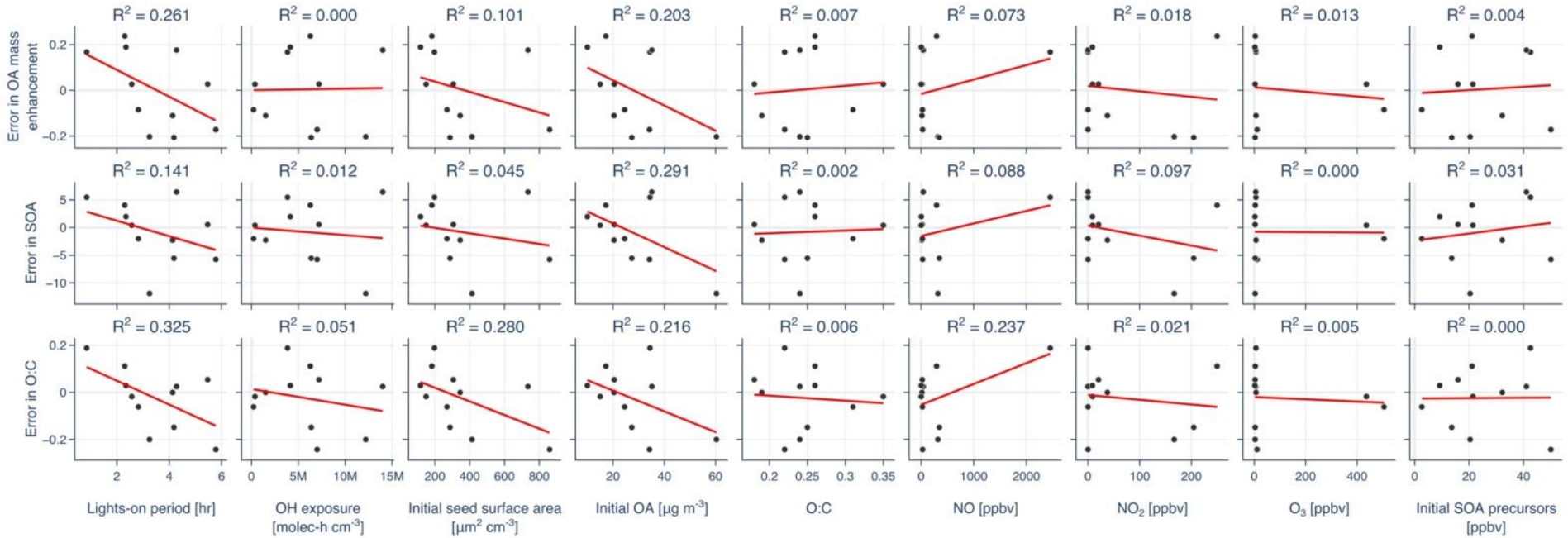

Figure S.19: Model error in OA mass enhancement ratio, SOA production, and OA O:C regressed against lights-on period, OH exposure, and initial concentrations of seed surface area, OA mass, O:C, NO, NO_2, O_3, and SOA precursors.

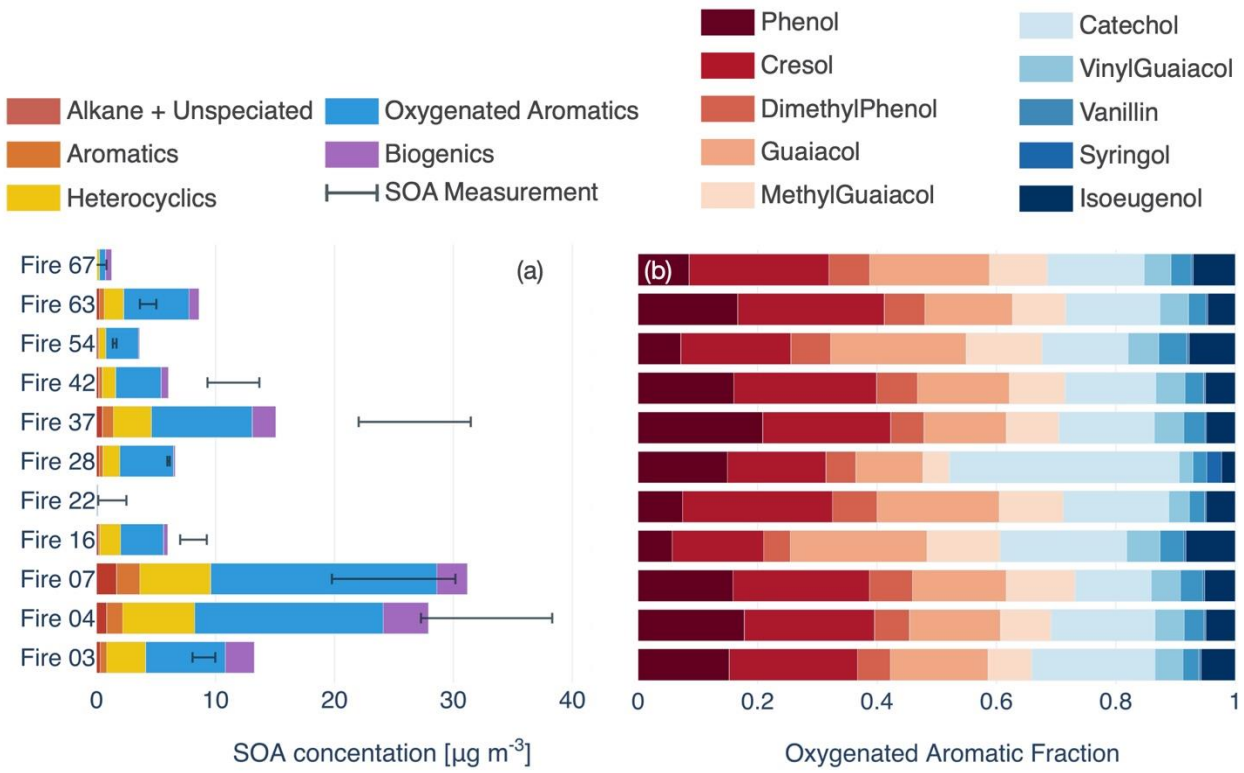

Figure S.20: (a) SOA mass concentrations apportioned by precursor class and (b) normalized precursor contributions to SOA arising from oxygenated aromatics. Data presented for all eleven chamber experiments.

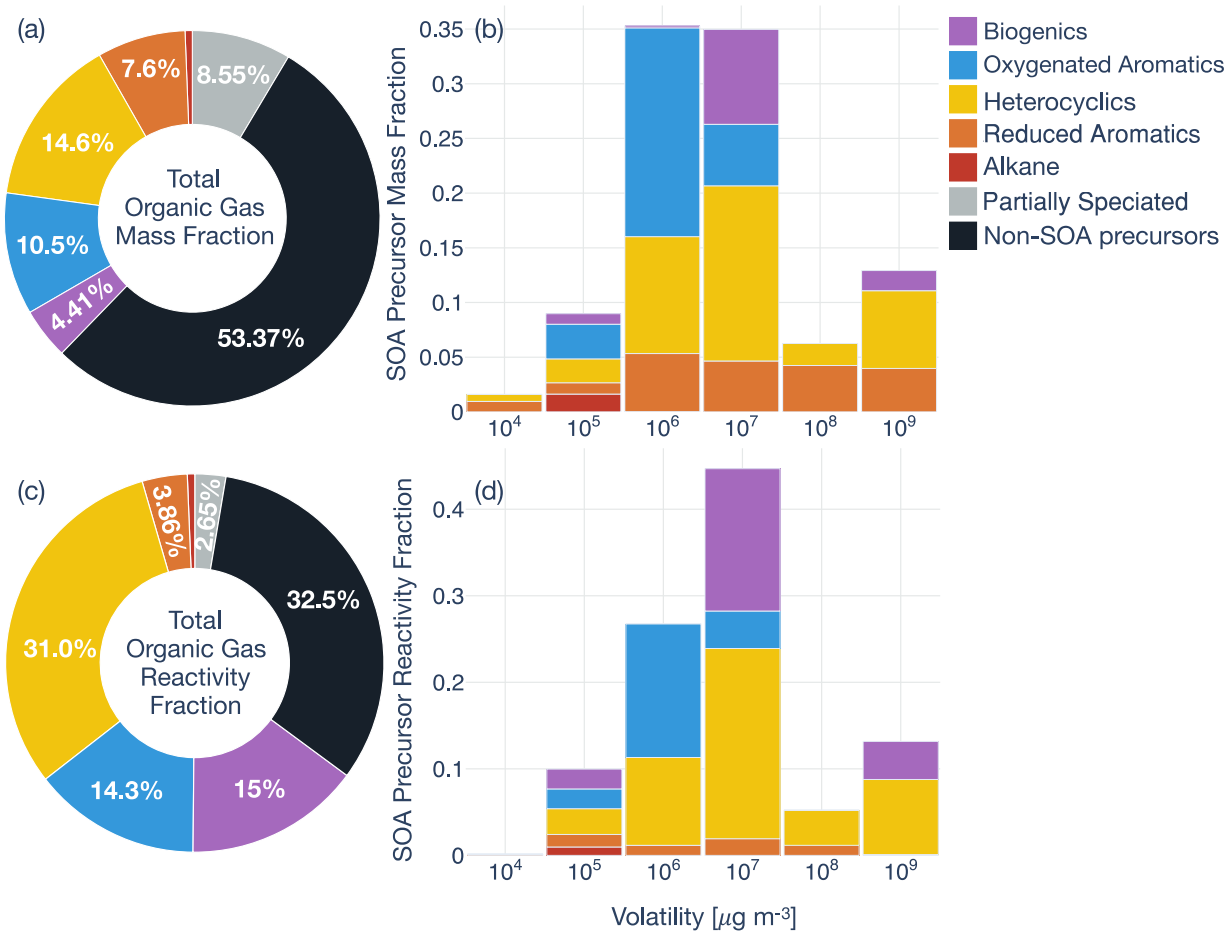

Figure S.21: (a) SOA precursor classes as a mass fraction of the total VOCs and (b) normalized distribution of SOA precursor emissions in volatility space. (c) SOA precursor classes as a fraction of the total VOC reactivity and (d) normalized distribution of SOA precursor reactivity in volatility space. Data are presented as an average of the emissions over the eleven chamber experiments.

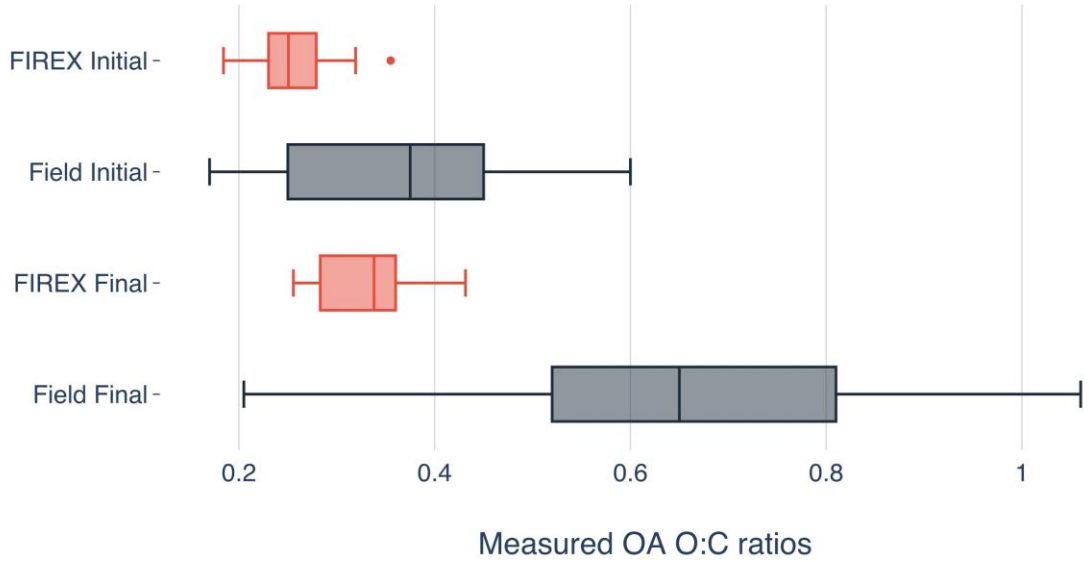

Figure S.22: Box plots for initial and final OA O:C ratios from the chamber experiments performed during FIREX and a host of field studies. The field studies are summarized in Hodshire et al.[13] The orange horizontal lines are medians and the dotted horizontal lines are means. Solid circles are outliers.

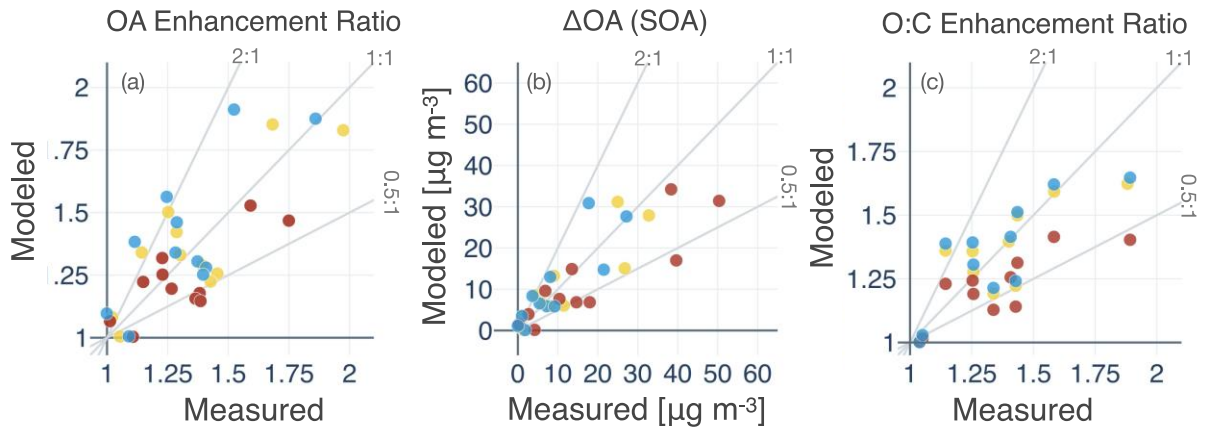

	Slope	intercept	R^2	RMSE	Slope	intercept	R^2	RMSE	Slope	intercept	R^2	RMSE
Base	0.79	0.29	0.68	0.161	0.80	1.62	0.79	4.97	0.70	0.38	0.67	0.122
SF = 0.5	0.57	0.47	0.61	0.104	0.60	1.347	0.80	5.41	0.45	0.60	0.67	0.082
SF = 1.0	0.92	0.18	0.58	0.194	0.98	1.52	0.74	5.46	0.70	0.39	0.67	0.128

Figure S.23: End-of-experiment model-measurement comparison for (a) OA mass enhancement ratios (ratio of final to initial particle-wall-loss-corrected OA mass), (b) SOA production (µg m^{-3}), and (c) OA O:C enhancement ratios (ratio of final to initial O:C ratios) for all eleven chamber experiments for three different assumptions about the scaling factor: constant scaling factor of 0.5 and 1 and a scaling factor as a function of the OA oxidation state.

References

(1) Middlebrook, A. M.; Bahreini, R.; Jimenez, J. L.; Canagaratna, M. R. Evaluation of Composition-Dependent Collection Efficiencies for the Aerodyne Aerosol Mass Spectrometer Using Field Data. Aerosol Sci. Technol. **2012**, 46 (3), 258–271.

(2) Tkacik, D. S.; Robinson, E. S.; Ahern, A.; Saleh, R.; Stockwell, C.; Veres, P.; Simpson, I. J.; Meinardi, S.; Blake, D. R.; Yokelson, R. J.; Presto, A. A.; Sullivan, R. C.; Donahue, N. M.; Robinson, A. L. A Dual-Chamber Method for Quantifying the Effects of Atmospheric Perturbations on Secondary Organic Aerosol Formation from Biomass Burning Emissions: Investigation of Biomass Burning SOA. J. Geophys. Res. D: Atmos. **2017**, 122 (11), 6043–6058.

(3) Lim, C. Y.; Hagan, D. H.; Coggon, M. M.; Koss, A. R.; Sekimoto, K.; Gouw, J. de; Warneke, C.; Cappa, C. D.; Kroll, J. H. Secondary Organic Aerosol Formation from the Laboratory Oxidation of Biomass Burning Emissions. Atmos. Chem. Phys. **2019**, 19 (19), 12797–12809.

(4) Loza, C. L.; Craven, J. S.; Yee, L. D.; Coggon, M. M.; Schwantes, R. H.; Shiraiwa, M.; Zhang, X.; Schilling, K. A.; Ng, N. L.; Canagaratna, M. R.; Ziemann, P. J.; Flagan, R. C.; Seinfeld, J. H. Secondary Organic Aerosol Yields of 12-Carbon Alkanes. Atmos. Chem. Phys. **2014**, 14 (3), 1423–1439.

(5) Ng, N. L.; Kroll, J. H.; Chan, A. W. H.; Chhabra, P. S.; Flagan, R. C.; Seinfeld, J. H. Secondary Organic Aerosol Formation from m-Xylene, Toluene, and Benzene. Atmos. Chem. Phys. **2007**, 7 (14), 3909–3922.

(6) Zhang, X.; Cappa, C. D.; Jathar, S. H.; McVay, R. C.; Ensberg, J. J.; Kleeman, M. J.; Seinfeld, J. H. Influence of Vapor Wall Loss in Laboratory Chambers on Yields of Secondary Organic Aerosol. Proc. Natl. Acad. Sci. U. S. A. **2014**, 111 (16), 5802–5807.

(7) Chhabra, P. S.; Ng, N. L.; Canagaratna, M. R.; Corrigan, A. L.; Russell, L. M.; Worsnop, D. R.; Flagan, R. C.; Seinfeld, J. H. Elemental Composition and Oxidation of Chamber Organic Aerosol. Atmos. Chem. Phys. **2011**, 11 (17), 8827–8845.

(8) Yee, L. D.; Kautzman, K. E.; Loza, C. L.; Schilling, K. A.; Coggon, M. M.; Chhabra, P. S.; Chan, M. N.; Chan, A. W. H.; Hersey, S. P.; Crounse, J. D.; Wennberg, P. O.; Flagan, R. C.; Seinfeld, J. H. Secondary Organic Aerosol Formation from Biomass Burning Intermediates: Phenol and Methoxyphenols. Atmos. Chem. Phys. **2013**, 13 (16), 8019–8043.

(9) He, Y.; King, B.; Pothier, M.; Lewane, L.; Akherati, A.; Mattila, J.; Farmer, D. K.; McCormick, R.; Thornton, M.; Pierce, J. R.; Volckens, J.; Jathar, S. H. Secondary Organic Aerosol Formation from Evaporated Biofuels: Comparison to Gasoline and Correction for Vapor Wall Losses. Environmental Sciences: Processes and Impacts **2020,** accepted.

(10) Koss, A. R.; Sekimoto, K.; Gilman, J. B.; Selimovic, V.; Coggon, M. M.; Zarzana, K. J.; Yuan, B.; Lerner, B. M.; Brown, S. S.; Jimenez, J. L.; Krechmer, J.; Roberts, J. M.; Warneke, C.; Yokelson, R. J.; Gouw, J. de. Non-Methane Organic Gas Emissions from Biomass Burning: Identification, Quantification, and Emission Factors from PTR-ToF during the FIREX 2016 Laboratory Experiment. Atmos. Chem. Phys. **2018**, 18 (5), 3299–3319.

(11) Kroll, J. H.; Donahue, N. M.; Jimenez, J. L.; Kessler, S. H.; Canagaratna, M. R.; Wilson, K. R.; Altieri, K. E.; Mazzoleni, L. R.; Wozniak, A. S.; Bluhm, H.; Mysak, E. R.; Smith, J. D.; Kolb, C. E.; Worsnop, D. R. Carbon Oxidation State as a Metric for Describing the Chemistry of Atmospheric Organic Aerosol. Nat. Chem. **2011**, 3 (2), 133–139.

(12) Coggon, M. M.; Lim, C. Y.; Koss, A. R.; Sekimoto, K.; Yuan, B.; Gilman, J. B.; Hagan, D. H.; Selimovic, V.; Zarzana, K. J.; Brown, S. S.; Roberts, J. M.; Müller, M.; Yokelson, R.; Wisthaler, A.; Krechmer, J. E.; Jimenez, J. L.; Cappa, C.; Kroll, J. H.; Gouw, J. de; Warneke, C. OH Chemistry of Non-Methane Organic Gases (NMOGs) Emitted from Laboratory and Ambient Biomass Burning Smoke: Evaluating the Influence of Furans and Oxygenated Aromatics on Ozone and Secondary NMOG Formation. Atmos. Chem. Phys. **2019**, 19 (23), 14875–14899.

(13) Hodshire, A. L.; Akherati, A.; Alvarado, M. J.; Brown-Steiner, B.; Jathar, S. H.; Jimenez, J. L.; Kreidenweis, S. M.; Lonsdale, C. R.; Onasch, T. B.; Ortega, A. M.; Pierce, J. R. Aging Effects on

Biomass Burning Aerosol Mass and Composition: A Critical Review of Field and Laboratory Studies. Environ. Sci. Technol. **2019**, 53 (17), 10007–10022.